Strongly vs. weakly associating anions: transport–structure relationship in LiTFSI–LiNO3 electrolytes

Ervin Rems, Tim Šlosar, Sara Drvarič Talian, Matej Huš, Robert Dominko, Alessandra Serva

Strongly vs weakly associating anions: Transport-structure relationship in LiTFSI-$LiNO_3$ electrolytes

Ervin Rems,[1,2,a)] Tim Šlosar,[1] Sara Drvarič Talian,[1] Matej Huš,[3,4] Robert Dominko,[1,2,5] and Alessandra Serva[6,7,b)]

[1)] *Department of Materials Chemistry, National Institute of Chemistry, Hajdrihova 19, SI-1001 Ljubljana, Slovenia*

[2)] *Faculty of Chemistry and Chemical Technology, University of Ljubljana, Večna pot 113, SI-1000 Ljubljana, Slovenia*

[3)] *Department of Catalysis and Chemical Reaction Engineering, National Institute of Chemistry, Hajdrihova 19, SI-1001 Ljubljana, Slovenia*

[4)] *Association for Technical Culture of Slovenia (ZOTKS), Zaloška 65, SI-1000 Ljubljana, Slovenia*

[5)] *ALISTORE - European Research Institute, FR CNRS 3104, 80039 Amiens Cedex, France*

[6)] *Sorbonne Université, CNRS, Physicochimie des Électrolytes et Nanosystèmes Interfaciaux, F-75005 Paris, France*

[7)] *Réseau sur le Stockage Electrochimique de l'Energie (RS2E), FR CNRS 3459, 80039 Amiens Cedex, France*

(Dated: 16 July 2025)

Liquid battery electrolytes based on mixtures of salts with weakly and strongly associating anions have emerged as a promising route toward high-performance, sustainable battery technologies. Their success is primarily attributed to the unique influence of salt composition on the solvation structure. Here, we employ classical molecular dynamics simulations, corroborated by experimental data, to study mixed lithium bis(trifluoromethanesulfonyl)imide (LiTFSI) / lithium nitrate ($LiNO_3$) in diglyme electrolytes, a formulation of particular interest for lithium–sulfur and lithium-oxygen batteries. We investigate how the ratio of weakly associating anions ($TFSI^-$) to strongly associating anions (NO_3^-) affects ion transport within the electrolyte. Our findings reveal that the anion ratio significantly impacts both the solvation structure and the solvation dynamics, which together contribute to the distinct transport behavior observed in these systems. These findings underscore the tunability of battery electrolyte transport properties through careful mixing of anions.

I. INTRODUCTION

The rapid commercial expansion of Li-ion batteries raises environmental, geopolitical, and ethical dilemmas.[1] To address these issues, novel battery electrode materials, such as lithium metal[2] and multivalent batteries,[3] have been proposed. As the electrolytes typically used in commercial Li-ion batteries are incompatible with these materials, their practical implementation depends critically on electrolyte design.[4]

In this context, mixing of salts with different anions appears as an increasingly promising approach.[5] Electrolytes with anions that differ in the anion–cation interaction strength are of particular interest due to their distinctive solvation structure.[6] Indeed, mixing strongly and weakly associating anions has been shown to enable enhanced stability and prolonged lifetime of Li metal[7] and Na metal[8] batteries. The important feature observed in these electrolytes is the large population of anions in the first Li^+ solvation shell, which modulates the electrochemical behavior of a battery cell. Despite advances in understanding their structure, the transport properties of such mixed-anion electrolytes have received limited attention. However, understanding transport properties is crucial, as ion transport governs cell polarization, affecting battery charging efficiency and lifespan.[9]

A prominent class of mixed-anion battery electrolytes is based on lithium bis(trifluoromethanesulfonyl)imide (LiTFSI) and lithium nitrate ($LiNO_3$) in organic solvents, significantly improving the performance of Li-S[10] and Li-O_2[11] batteries. In these systems, $TFSI^-$ exhibits weak association with Li^+, whereas NO_3^- associates strongly.[12,13] The origin of the improved performance of Li-S batteries with electrolytes containing strongly associating NO_3^- anions is complex and not fully understood.[14]

Chu *et al.* have systematically investigated the performance of Li-S battery cells with LiTFSI-$LiNO_3$ in 1,3-dioxolane (DOL) - 1,2-dimethoxyethane (DME) electrolyte, varying the $TFSI^-$ to NO_3^- ratio at a constant total salt concentration of 1 M.[15] The $TFSI^-$ to NO_3^- anion concentration ratio has been identified as a critical parameter governing sulfur species solubility and electrolyte electrochemical stability, both of which contribute to improved battery performance. This enhancement has been primarily attributed to changes in the electrolyte structure, specifically the increased presence of strongly associating NO_3^- ions in the Li^+ solvation shell. However, the effect of the interplay between weakly associating $TFSI^-$ and strongly associating NO_3^- ions on the ion transport

[a)] Electronic mail: ervin.rems@ki.si
[b)] Electronic mail: alessandra.serva@sorbonne-universite.fr

through the electrolyte remains unclear.

In this work, we employ classical molecular dynamics (MD) simulations, supported by experimental validation, to systematically investigate the effect of the concentration ratio between strongly and weakly associating anions on the transport properties of a representative model electrolyte: LiTFSI-$LiNO_3$ in diglyme (G2) at a 1.49 mol kg^{-1} molality. We choose G2 for its established role as a solvent in Li–S battery electrolytes,[10,16] while the selected salt molality reflects typical concentrations used in practical cell configurations.[11,15,17] First, we establish the effect of anions ratio on two key descriptors of ion transport: ionic conductivity and Li^+ transference number. Next, we discuss correlations in ionic movements to understand the non-ideal transport properties of these electrolytes. Finally, we establish that a cooperative action of Li^+ solvation structure and Li^+ solvation dynamics, which both heavily depend on the $TFSI^-$:NO_3^- ratio, provides a rationale for the observed ion-ion correlations.

II. METHODS

A. Classical molecular dynamics simulations

Classical MD simulations were performed using LAMMPS.[18] Simulated systems were composed of 500 G2 molecules and a varying number of Li^+, $TFSI^-$, and NO_3^- ions. The corresponding chemical formulae are shown in Figure 1. Mixed LiTFSI-$LiNO_3$ systems were simulated as a function of the $TFSI^-$:NO_3^- ratio, keeping the total concentration fixed at 1.49 mol kg^{-1} (see Table I for the details). Additional simulations of single-anion LiTFSI in G2 and $LiNO_3$ in G2 as a function of the salt concentration were also performed (Table S1). The Li^+ cation was represented by the Åqvist force field,[19] the $TFSI^-$ anion by the CL&P[20] model, the NO_3^- anion by the revisited OPLS-2009IL[21] model, and G2 by OPLS all-atom[22] model. The net charge of the ions was scaled by 0.8 to mimic polarization effects and improve the description of transport properties.[23–25] A cut-off of 12 Å was applied for non-bonded interactions, while the particle-particle particle-mesh method was used to evaluate electrostatic energies at the relative force error of 10^{-5}. C−H bonds of G2 were kept rigid using the SHAKE algorithm. The timestep was set to 1 fs. The initial configurations were generated by randomly distributing particles in a cubic box using PACKMOL,[26] followed by energy minimization. The system was first equilibrated for 5 ns in the isothermal–isobaric (NpT) ensemble at 298.15 K and 1 atm to reach a constant density. The average volume of the system was evaluated between 1 ns and 5 ns of the NpT simulation. The densities obtained from simulations agree well with experimental values (see Table S2 for some of the simulated systems), with errors below 0.4%. A second equilibration was performed in the canonical ensemble (NVT) at 298.15 K for 10 ns. Finally, production NVT simulation at 298.15 K was performed for 90 ns. The trajectory was saved every 1 ps. The temperature and pressure were controlled using the Nosé-Hoover thermostat and barostat with relaxation times of 100 fs and 1000 fs, respectively. LAMMPS input files were generated using a modified version of fftool.[27] Trajectories were analyzed using TRAVIS,[28,29] MDAnalysis,[30,31] SolvationAnalysis,[32] mean_square_displacements utility,[33] and self-written tools. Solvation networks were visualized using NGLview.[34]

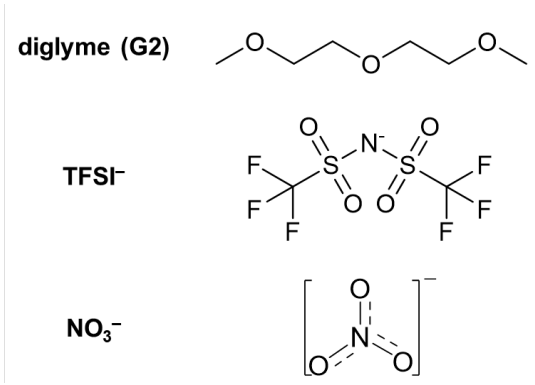

FIG. 1. **Structural formulae of G2, $TFSI^-$, and NO_3^-.**

$x(NO_3^-)$	N(G2)	$N(Li^+)$	$N(TFSI^-)$	$N(NO_3^-)$	l/Å	ρ/g cm^{-3}
0.0	500	100	100	0	52.14	1.12
0.2	500	100	80	20	51.64	1.10
0.4	500	100	60	40	51.14	1.08
0.5	500	100	50	50	50.86	1.07
0.6	500	100	40	60	50.61	1.06
0.8	500	100	20	80	50.10	1.03
1.0	500	100	0	100	49.58	1.01

TABLE I. Composition of the simulated mixed-anions electrolytes (x being the molar faction and N the number of species) together with box edge length, l, and density, ρ, obtained from a NpT simulation.

B. Experimental measurements

Electrolytes were prepared from previously dried salt and solvents: diglyme (Acros Organics, 99%, extra pure) was dried using 4 Å molecular sieves, refluxed overnight with a Na/K alloy, and purified by fractional distillation, $LiNO_3$ (Merck, 99.995%) was dried at 150 °C overnight in vacuum, and LiTFSI (Sigma-Aldrich, 99.95%) was dried at 140 °C overnight in vacuum.

The density was measured at 298.15 K and atmospheric pressure with a vibration-type density meter, the Anton Paar DMA 500 with a declared reproducibility of 1.10 kg m^{-3}. The calibration of the densimeter was performed using the density data of milipore water.

Raman spectroscopy measurements were performed using a Ram II Raman spectrometer with a 785 nm laser by averaging 200 samplings in the 50 cm^{-1} to 3600 cm^{-1}

range.

For transference number determination, Li metal (Gelon, 200 µm thickness) symmetrical cells were assembled under Ar atmosphere (MBraun glovebox, O_2 and $H_2O < 1$ ppm). Two 2 cm^2 Li electrodes, 9 layers of Celgard separators and 100 µL of electrolyte were used for cell assembly and the cell was packaged in a Triplex foil packaging (PE 90 µm/Al 10 µm/PET 20 µm) with Ni contact strips. The cells were assembled and left for 7 days to stabilize. Low-frequency electrochemical impedance spectroscopy (EIS) spectra were measured using VMP3-e BioLogic potentiostat/galvanostat (1 MHz–0.1 mHz, 10 mV rms amplitude). For the determination of ionic conductivity, symmetric cells were assembled using the same pouch cell casings, two stainless steel blocking electrodes (16 mm in diameter), one Celgard 2320 separator layer and 20 µL of the chosen electrolyte. EIS spectra of these cells were measured in a frequency range of 1 MHz to 1 kHz at 298.15 K. The resistive intercept was extracted from the spectra. Furthermore, the EIS spectrum of a cell with LP40 electrolyte (1 M $LiPF_6$ in 1/1 wt/wt diethyl carbonate/ethylene carbonate) was measured to provide a reference value and allow calculation of the ionic conductivity. The conductivity of the LP40 electrolyte was assumed to be 8.0 mS cm^{-1}.[35] The error in the ionic conductivity was below 0.5 mS cm^{-1}.

III. RESULTS AND DISCUSSION

A. Ionic conductivity and Li^+ transference number

The key transport features of a battery electrolyte are the ionic conductivity, σ, and the Li^+ transference number, t_+. We start by investigating how the $TFSI^-$:NO_3^- ratio affects these two properties.

The ionic conductivity quantifies the mobility of ions involved in electrochemical reactions, influencing the power output of the battery cell.[36] We evaluate it from the MD trajectory through

$$\sigma = \frac{e_0}{k_B T V} \lim_{t\to\infty} \frac{1}{6t} \left\langle \left| \sum_i q_i(\overrightarrow{r_i(t)} - \overrightarrow{r_i(t_0)}) \right|^2 \right\rangle \qquad (1)$$

where e_0 is the elementary charge, k_B the Boltzmann constant, T the temperature, V the volume, t the time, q_i the formal charge of an ion i, and $\vec{r_i}$ its cartesian coordinates. Note that this equation accounts for the effect of all ion correlations.

Figure 2a shows the ionic conductivity of the mixed-anions system at a 1.49 mol kg^{-1} total salt molality and various $TFSI^-$:NO_3^- ratios. Both in simulation and experiment, the conductivity monotonically decreases with an increasing proportion of NO_3^- anions. While the simulation adequately describes the experimental trend, the match is not quantitative, as expected for simulations based on a classical non-polarisable force field.[37,38]

A similar trend in conductivity was observed experimentally in solutions based on a triethyl phosphate solvent, where σ of 1 M LiTFSI solution (4.79 mS cm^{-1}) was 74 % higher than that of 1 M $LiNO_3$ solution (2.76 mS cm^{-1}).[39] Notably, the decrease in conductivity in mixed-anion electrolytes is relatively small, compared to the substantially lower conductivity for the $x(NO_3^-) = 1.0$ system. Similarly, only a slight decrease in σ was experimentally observed in liquid organic electrolytes containing lithium bis(fluorosulfonyl)imide (LiFSI) when mixed with strongly associating anions such as ClO_4^- or BF_4^-, albeit at low concentrations of strongly associating anions.[7,13]

In Figure S2a, we additionally examine the conductivity of single-anion solutions of LiTFSI and $LiNO_3$ in G2 at concentrations ranging from 0.30 mol kg^{-1} to 1.49 mol kg^{-1}. We observe that σ of the LiTFSI solutions is systematically higher than that of the $LiNO_3$ solutions. This is consistent with the experimental observation that a weaker interaction between the Li^+ cation and the salt anion correlates with a higher ionic conductivity of Li^+ electrolytes.[40] Similarly, LiTFSI

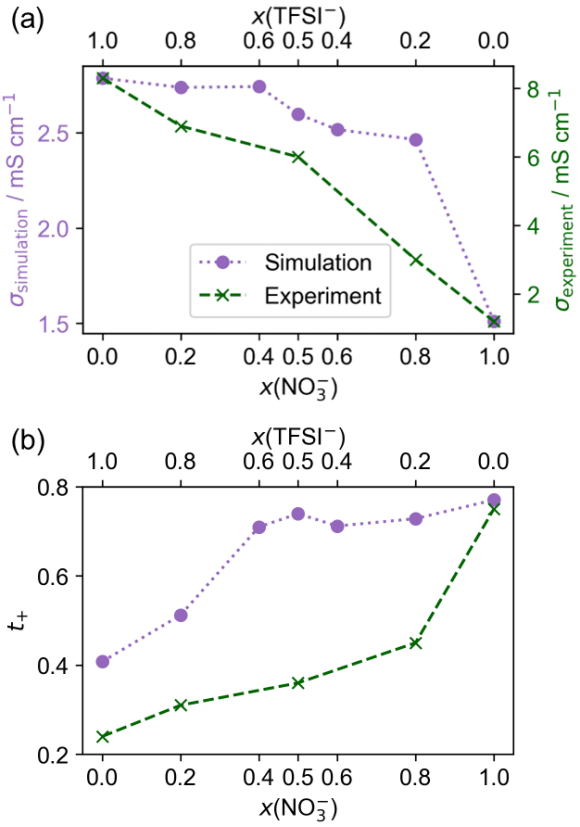

FIG. 2. **Transport properties of mixed LiTFSI-$LiNO_3$ in G2 solutions as a function of $TFSI^-$:NO_3^- ratio and fixed total molality of** 1.49 **mol kg^{-1}.** (a) Ionic conductivity, σ; (b) Li^+ transference number, t_+. MD simulation and experimental results are shown in purple and dark green, respectively.

electrolytes reach their maximum σ at a higher concentration than $LiNO_3$ (1.20 mol kg^{-1} vs 0.75 mol kg^{-1}).

The Li^+ transference number t_+ quantifies the fraction of the conductivity that is useful for the electrochemical reaction.[36] We compute t_+ from MD simulations as

$$t_+ = \frac{D^c_+ D^c_- - \left(D^c_{+-}\right)^2}{D^c_- \left(D^c_+ + D^c_- - 2D^c_{+-}\right)} \tag{2}$$

where + and − denote cations and anions, respectively, and D^c is the corresponding collective diffusion coefficient. The calculation of collective diffusion coefficients is detailed in III B. This expression for t_+ was derived by Wohde *et al.* from the Onsager reciprocal relations and the linear response theory, and takes into account all correlations between ionic movements.[41] Experimentally, we determine the t_+ from low-frequency EIS spectra (Figure S1) as

$$t_+ = \frac{R_{el}}{R_{el} + R_W} \tag{3}$$

where R_{el} and R_W are the resistive intercept and the resistance of diffusion acrs, respectively.[41]

t_+, shown in Figure 2b, increases as the amount of NO_3^- anions increases, both in simulations and experiments. Similarly, a high (0.49) and low (0.32) t_+ were observed for 1 M $LiNO_3$ and 1 M $LiPF_6$ salts, respectively, in dimethyl sulfoxide-propylene carbonate solvent,[42] where PF_6^- anions, like $TFSI^-$, exhibit considerably weaker anion association strength than NO_3^-.[12] We also study the effect of concentration on t_+ in single-anion electrolytes (Figure S2b). The t_+ for LiTFSI and $LiNO_3$ electrolytes almost coincide at the lowest concentration (0.30 mol kg^{-1}). However, as the salt concentration increases, t_+ decreases for LiTFSI and increases for $LiNO_3$. At 1.49 mol kg^{-1}, a striking difference in t_+ is observed between the two salts (0.41 for LiTFSI vs 0.77 for $LiNO_3$).

The behavior observed in the presence of strongly associating NO_3^- anions resembles the transport characteristics of solvent-in-salt electrolytes, where a reduced σ is coupled with a large t_+.[43] A similar coupling of ionic conductivity and Li^+ transference number was observed in MD simulations of 0.88 M LiTFSI and 0.33 M LiTFSI + 0.66 M $LiNO_3$, both in a mixture of 1,2-dimethoxyethane and 1,3-dioxolane.[44] Carefully exploring the chemical and concentrational space in mixed-anion electrolytes thus represents an interesting avenue for boosting the transport properties.

B. Correlations in ion transport

In an ideal electrolyte, the ionic conductivity is proportional to the molar concentration of ions (charge carriers). As the total molar concentration of ions in the investigated systems does not vary, the decrease of σ in solutions with larger amounts of NO_3^- anions suggests a strong deviation from the ideal behavior.

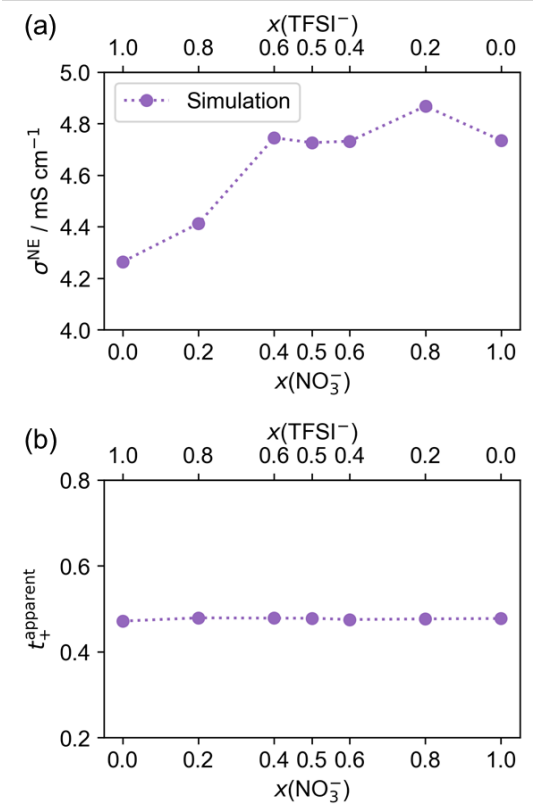

FIG. 3. **The ideal electrolyte behavior fails to capture the transport trends.** (a) Nernst-Einstein conductivity, σ^{NE}, and (b) apparent Li^+ transference number, $t_+^{apparent}$, for mixed LiTFSI-$LiNO_3$ in G2 solutions as a function of $TFSI^-$:NO_3^- ratio and fixed total molality of 1.49 mol kg^{-1}.

The degree of non-ideality can be quantified from the simulation trajectory. Specifically, σ and t_+, which account for the correlated movements of ions, can be simplified and expressed in terms of self-diffusion coefficients, D^s, if an ideal electrolyte is assumed. This yields the Nernst-Einstein conductivity, σ^{NE},

$$\sigma^{NE} = \frac{e_0}{k_B T V} \sum_i N_i q_i^2 D_i^s \tag{4}$$

where N_i, q_i, D_i^s are the number, the formal charge, and the self-diffusion coefficient of an ionic species i. Here, the species is either Li^+, $TFSI^-$, or NO_3^-. The calculation of self-diffusion coefficients is detailed in III B. Similarly to σ^{NE}, the apparent Li^+ transference number, $t_+^{apparent}$, can be defined for an ideal electrolyte

$$t_+^{apparent} = \frac{D_+^s}{D_+^s + D_-^s} \tag{5}$$

where + and − denote cations and anions, respectively, and D^s is the corresponding self-diffusion coefficient.

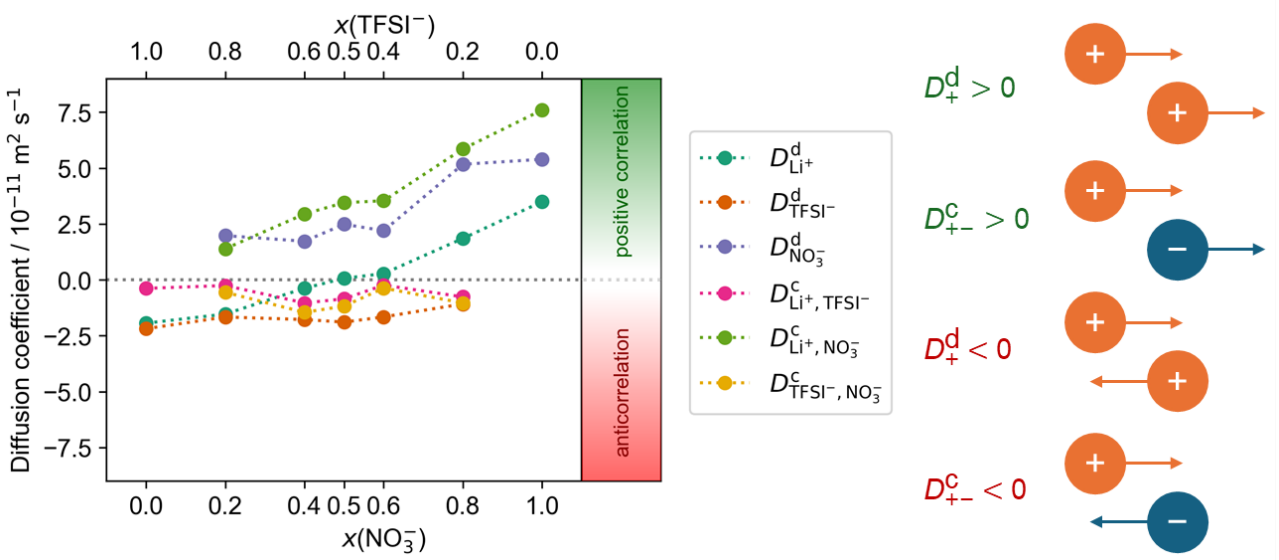

FIG. 4. **Ion-Ion correlation effects**. Distinct, D^{d}, and collective, D^{c}, diffusion coefficients in mixed LiTFSI-$LiNO_3$-G2 electrolytes as a function of the TFSI:NO_3 ratio at a fixed total molality of 1.49 mol kg^{-1}. Large positive and large negative values indicate strong positive correlation and anticorrelation, respectively. The meaning of diffusion coefficients is illustrated on the left. Cations and anions are represented in orange and teal blue, respectively. Arrows illustrate the relative direction of the movement, with ions moving preferentially in the same direction and in the opposite directions for positively correlated and anticorrelated movement, respectively.

σ^{NE} and t_+^{apparent} are reported in Figure 3 and Figure S3 for the mixed-anions and single-anion electrolytes, respectively. It is evident that these metrics deviate significantly from σ and t_+. As expected, this deviation is more pronounced in electrolytes containing NO_3^- anions, where stronger interactions between cations and anions more significantly affect the dynamics. Importantly, assuming an ideal behavior in such cases could lead to qualitatively different conclusions. Specifically, σ^{NE} increases by increasing the $TFSI^-$:NO_3^- ratio, whereas σ decreases. Additionally, t_+^{apparent} remains relatively unchanged across different systems, whereas t_+ is strongly affected. A similar behavior of t_+^{apparent} and t_+ was observed for the LiTFSI water-in-salt electrolyte.[25]

This discrepancy highlights the important role of correlated ion movements in transport phenomena within the investigated electrolytes. It reinforces the importance of considering complex correlations in the molecular modeling of battery electrolytes[45] and motivates a deeper investigation of ion-ion correlations in our systems.

Correlated movements between two distinct species A and B are quantified by the collective diffusion coefficient $D^{\mathrm{c}}_{\mathrm{AB}}$:

$$D^{\mathrm{c}}_{\mathrm{AB}} = \frac{1}{\sqrt{N_{\mathrm{A}}N_{\mathrm{B}}}} \lim_{t\to\infty} \frac{1}{6t} \left\langle \sum_i^{N_{\mathrm{A}}} (\overrightarrow{r_i(t)} - \overrightarrow{r_i(t_0)}) \sum_j^{N_{\mathrm{B}}} (\overrightarrow{r_j(t)} - \overrightarrow{r_j(t_0)}) \right\rangle \quad (6)$$

In other words, $D^{\mathrm{c}}_{\mathrm{AB}}$ describes how correlated transport of species A and B is.[46] Specifically, $D^{\mathrm{c}}_{\mathrm{AB}} < 0$, $D^{\mathrm{c}}_{\mathrm{AB}} = 0$, and $D^{\mathrm{c}}_{\mathrm{AB}} > 0$ correspond to anticorrelated, uncorrelated, and positively correlated movements of species A and B, while $|D^{\mathrm{c}}_{\mathrm{AB}}|$ indicates the magnitude of this (anti)correlation.

For chemically identical species (A = B), this relation reads:

$$D^{\mathrm{c}}_{\mathrm{A}} = \frac{1}{N_A} \lim_{t\to\infty} \frac{1}{6t} \left\langle \left| \sum_i^{N_{\mathrm{A}}} (\overrightarrow{r_i(t)} - \overrightarrow{r_i(t_0)}) \right|^2 \right\rangle \quad (7)$$

On the other hand, the self-diffusion coefficient $D^{\mathrm{s}}_{\mathrm{A}}$ treats movements of particles independently:

$$D^{\mathrm{s}}_{\mathrm{A}} = \lim_{t\to\infty} \frac{1}{6t} \left\langle \left| (\overrightarrow{r_i(t)} - \overrightarrow{r_i(t_0)}) \right|^2 \right\rangle \quad (8)$$

D^{s} of all ionic species is reported in Figure S4 for all investigated electrolytes. The descriptor of correlations is the distinct diffusion coefficient, $D^{\mathrm{d}}_{\mathrm{A}}$:

$$D^{\mathrm{d}}_{\mathrm{A}} = D^{\mathrm{c}}_{\mathrm{A}} - D^{\mathrm{s}}_{\mathrm{A}} \quad (9)$$

The meaning of $D^{\mathrm{d}}_{\mathrm{A}}$ is analogous to that of $D^{\mathrm{c}}_{\mathrm{AB}}$.

The relevant D^{d} and D^{c} for mixed-anion electrolytes are shown in Figure 4. Strong positive correlations are observed in systems containing NO_3^-anions, for both $D^{\mathrm{d}}_{NO_3^-}$ and $D^{\mathrm{c}}_{Li^+,NO_3^-}$, which intensify at increased NO_3^- concentrations. Conversely, the corresponding

coefficients for the $TFSI^-$ anion ($D^{d}_{TFSI^-}$ and $D^{c}_{Li^+,TFSI^-}$) exhibit weak anticorrelations. In particular, the self-anticorrelation of $TFSI^-$ is notable, while the Li^+—$TFSI^-$ cross-anticorrelation is small. This is in agreement with experimentally observed anticorrelated transport between Li^+–$TFSI^-$, Li^+–Li^+, and $TFSI^-$–$TFSI^-$ ion pairs in tetraglyme-based electrolytes.[47] The degree of anticorrelation in Li^+–$TFSI^-$ transport was reported to be substantially lower than that of Li^+–Li^+ and $TFSI^-$–$TFSI^-$,[47] consistent with our results. Further, for $D^{d}_{Li^+}$, we note a transition from anticorrelated to positively correlated transport: Li^+ transport is anticorrelated in systems enriched with $TFSI^-$ ions, positively correlated in those enriched with NO_3^-, and uncorrelated when $m(\mathrm{LiTFSI}) \approx m(\mathrm{LiNO_3})$.

A similar behavior is observed in single-anion electrolytes (Figure S5). Regardless of the salt concentration, *(i)* both Li^+ and anion transport are anticorrelated in LiTFSI electrolytes and positively correlated in $LiNO_3$ electrolytes; *(ii)* the transport of Li^+ and anions is positively correlated; *(iii)* all (anti)correlations are stronger in $LiNO_3$ compared to LiTFSI electrolytes.

To conclude, the presence of NO_3^- anions leads to pronounced ion correlations, whereas such effects are significantly weaker in $TFSI^-$-dominated electrolytes. This aligns with the greater deviation of σ from σ^{NE} observed in $LiNO_3$ electrolytes compared to LiTFSI, a trend that is clearly reflected in the increase in the Haven ratio, H_R (Figure S6).[46] The likely explanation lies in the stronger Li^+–anion correlations associated with NO_3^- anions than with $TFSI^-$, which could arise from either: *(i)* a larger population of contact ion pairs or aggregates (structural origin); *(ii)* a longer lifetime of contact ion pairs or aggregates (dynamic origin).

C. Structural origin of ion correlations

We first study how the (average) local Li^+ solvation environment depends on the mixing of weakly and strongly associating anions. The coordination number between Li^+ and the oxygen (O) atoms of G2 is shown in Figure 5a. When only $TFSI^-$ anions are present, Li^+ ions are directly coordinated with 6 O atoms of G2, in accordance with previous classical MD simulations of the LiTFSI-G2 electrolyte (even though based on different force field parameters).[48] On the other hand, only 4 O atoms of G2 are directly coordinated to Li^+ in the $LiNO_3$-G2 electrolyte. In systems containing both anions, a clear monotonic trend is observed, in which an increase in the concentration of NO_3^- correlates with a lower coordination of Li^+ with the O(G2) atoms.

The coordination of the O atoms of NO_3^- to Li^+ is also shown in Figure 5a. A substantial number of NO_3^- anions occupy the first solvation shell of Li^+, and their presence increases with increasing concentration of NO_3^-, in accordance with decreased solvation with G2. Although Li^+ is coordinated, in total, with approximately six O atoms in all electrolytes, the G2 to NO_3^- ratio within the Li^+ solvation shell is governed by the $TFSI^-$ to NO_3^- ratio. In all cases, no short-range ordering of Li^+ and $TFSI^-$ ions is observed. These trends are similar to those observed for LiTFSI-$LiNO_3$ in tetraglyme[11] and DOL-DME.[15]

We use Raman spectroscopy to experimentally validate the simulated Li^+ solvation structure. The most informative regions of the Raman spectra are shown in Figure 5b, while the full spectra are provided in Figure S8. The ~ 880 $\mathrm{cm^{-1}}$ band is attributed to a distinct G2 conformation, corresponding to G2 molecules coordinated to Li^+.[49] The intensity of this band decreases with increasing $x(NO_3^-)$, confirming the decrease in G2 coordination number from MD. The symmetrical stretching vibration of NO_3^- is observed as a Raman band around 1040 $\mathrm{cm^{-1}}$. The formation of Li^+—NO_3^- contact ion pairs shifts this band ~ 5 $\mathrm{cm^{-1}}$ upward.[50] As the concentration of NO_3^- increases, the peak shifts toward higher wavenumbers, confirming a systematic increase in the amount of NO_3^- in the Li^+ solvation shell. In contrast, the position of the ~ 740 $\mathrm{cm^{-1}}$ band, associated with expansion–contraction of $TFSI^-$, remains unchanged. This aligns with the simulation result that $TFSI^-$ does not interact with Li^+, as such interaction would result in a comparable upward shift.[51,52]

How are G2 and NO_3^- coordinated to Li^+? While all O atoms of a G2 molecule are typically coordinated to a Li^+ ion, this is not the case for NO_3^-. This can be appreciated via the radial distribution functions (RDFs) and the coordination numbers shown in Figures 5c and 5d. RDFs between Li^+ and the center of mass (COM) of G2 exhibit a narrow, single peak, corresponding to tridentate binding of G2 via O atoms (a representative snapshot is shown in Figure S7). On the other hand, two distinct peaks are observed in Li^+-COM(NO_3^-) RDFs, suggesting monodentate and bidentate binding modes. Their relative contribution is evaluated in the inset of panel 5d, as described in Supplementary Note S1. Monodentate NO_3^- coordination is preferred, occurring at 5–7 times the frequency of bidentate coordination, with the exact ratio varying according to the electrolyte composition (Table S3). Electrolytes containing only NO_3^- anions exhibit a concentration-dependent increase in monodentate coordination, while no systematic variation is observed in mixed-anion systems with differing $TFSI^-$:NO_3^- ratios.

To get further insights into the Li^+ environment, a population analysis of Li^+ solvation clusters is shown in Figure 6a. Overall, the two dominant solvation clusters across the investigated electrolytes are: *(i)* Li^+ solvated with two G2 molecules ($[Li(G2)_2]^+$) and *(ii)* Li^+ solvated with one G2 molecule and two NO_3^- anions ($[Li(G2)(NO_3)_2]^-$). In particular, all Li^+ appear fully solvated with G2 in the 1.49 mol $\mathrm{kg^{-1}}$ LiTFSI electrolyte. However, with increasing number of NO_3^- anions in the system, a significant population

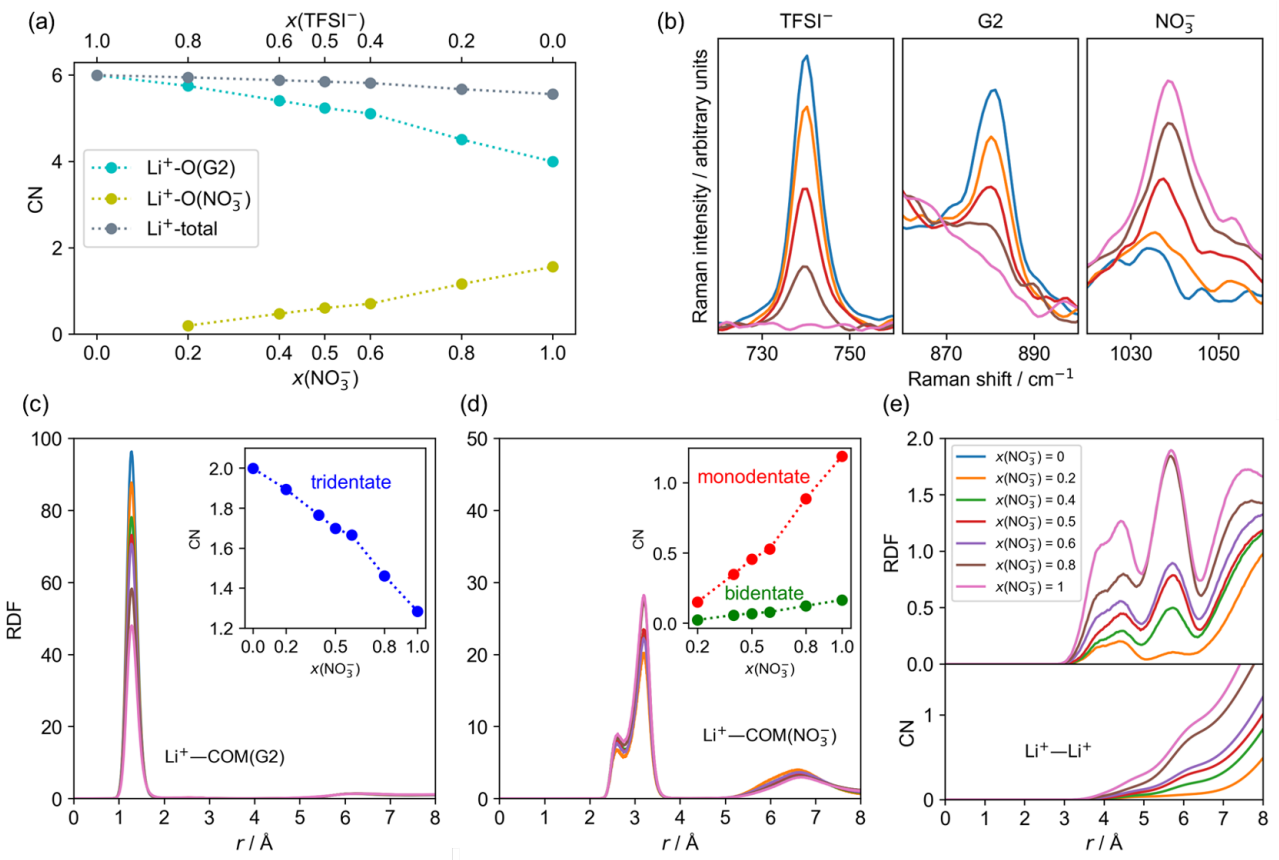

FIG. 5. **Structural origin of ion correlations in LiTFSI-$LiNO_3$ in G2 for different $TFSI^-$:NO_3^- ratios at fixed total molality of** 1.49 **mol** kg^{-1}**: Li^+ first solvation shell and beyond.** (a) Coordination numbers (CN), computed from the corresponding radial distribution functions (RDFs). The cut-off used is 3.6 Å for Li^+-O(G2) and 2.8 Å for Li^+-O(NO_3^-). (b) Selected regions of Raman spectra. The color of each curve corresponds to the electrolyte composition according to the legend in (e). Raman intensities are not comparable across the three regions. (c) RDF between Li^+ and center of mass (COM) of G2 and corresponding coordination number (for a cut-off of 2.1 Å, inset). (d) RDF between Li^+ and COM of NO_3^- and corresponding coordination number (inset). Red and green curve of the inset correspond to monodentate and bidentate coordination of NO_3^-. (e) Li^+-Li^+ RDF (top) and corresponding running coordination number (bottom).

of $[Li(G2)(NO_3)_2]^-$ clusters is observed. Notably, in the 1.49 mol kg^{-1} $LiNO_3$ electrolyte, $[Li(G2)(NO_3)_2]^-$ clusters become more common than $[Li(G2)_2]^+$ clusters. Additionally, no $TFSI^-$ anions are present in the observed solvation clusters, in agreement with the Li^+—$TFSI^-$ coordination number and Raman spectroscopy.

The Li^+—Li^+ RDFs and running coordination number (Figure 5e) indicates cation—cation structuring in NO_3^--containing electrolytes, implying formation of ion aggregates. To systematically investigate possible ion aggregation, we analyze ion *networks* in the electrolytes. An ion network is defined as a topological object composed of directly linked ions - in this case Li^+, $TFSI^-$, and NO_3^-. We also attribute *size* to every network: the number of Li^+ ions present in a network. Additionally, size 0 is attributed to every Li^+ ion that is not part of any network, i.e., is fully solvated with G2 molecules. The definition of a network size is chosen so that it best reflects the topological environments of Li^+ cations. Illustratively, we provide examples of network structures and corresponding network sizes in Figure 6b.

Networks composed of Li^+ and NO_3^- ions are observed in all electrolytes containing NO_3^-, while no $TFSI^-$ ions are present in the networks. Figure 6c shows the share of Li^+ ions as a function of the network size. A higher concentration of NO_3^- anions (at the account of lower concentration of $TFSI^-$) results in larger populations of networked Li^+. This is due to both *(i)* a larger population of ion networks and *(ii)* a larger size of ion networks. The presence of large aggregates composed of Li^+ and NO_3^- ions is in agreement with large populations of $[Li(G2)(NO_3)_2]^-$ clusters, as non-terminal networked Li^+ ions must be directly bound to at least two NO_3^- ions.

Similar trends as in mixed-anion electrolytes are observed for single-anion electrolytes. Li^+ ions are fully solvated by G2 molecules in all LiTFSI-based electrolytes, whereas more NO_3^- anions are found in

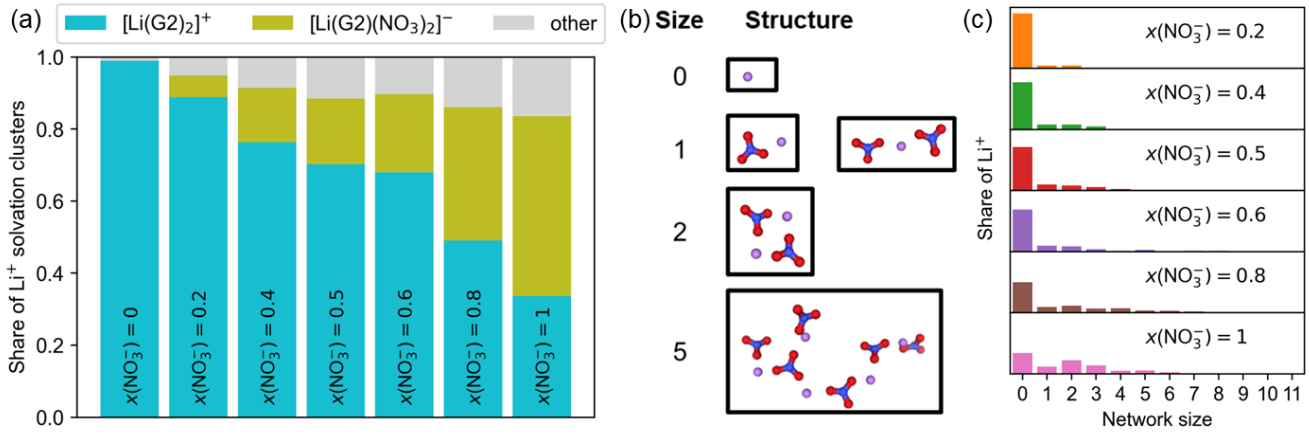

FIG. 6. **Structural origin of ion correlations in LiTFSI-$LiNO_3$ in G2 for different $TFSI^-$:NO_3^- ratios at fixed total molality of 1.49 mol kg^{-1}: Li^+ first solvation shell and beyond.** (a) Li^+ solvation cluster population analysis. (b) Illustration of ionic networks and the corresponding network sizes. Li^+ ions are shown in purple, while N and O atoms of NO_3^- ions are shown in blue and red, respectively. For visual clarity, G2 molecules are not shown. (c) Share of Li^+ ions present in networks of corresponding size.

the Li^+ solvation shell with rising salt concentration in $LiNO_3$ electrolytes (Figure S9). Analysis of ion networks confirms that network formation with Li^+ is exclusive to NO_3^- anions, and that the proportion of Li^+ ions participating in such networks increases with salt molality (Figure S10).

The transport properties observed in Section III A-III B can now be rationalized in terms of the electrolyte structure. An increasing proportion of NO_3^- anions leads to a greater number of NO_3^- in the first Li^+ solvation shell. This results in more correlated Li^+–NO_3^- movements (higher $D^c_{Li^+,NO_3^-}$). Similarly, the substantial amount of Li^+ present in the form of networks/aggregates of Li^+ and NO_3^- anions is likely the reason behind large, positive values of $D^d_{Li^+}$ and $D^d_{NO_3^-}$ in NO_3^--rich electrolytes. In the absence of such contact ion pairs and aggregates, i.e., in $TFSI^-$-rich electrolytes, a slightly anticorrelated ion transport is observed. This explains the transition from anticorrelated to positively correlated Li^+ transport when weakly associating $TFSI^-$ anions are replaced with strongly associating NO_3^- anions.

D. Dynamic origin of ion correlations

Correlations in ion transport may also be linked to the dynamics of the Li^+ solvation shell. For instance, if Li^+ is, on average, directly coordinated with a substantial number of NO_3^- anions, significant correlated transport will occur only if these ion pairs persist over timescales relevant to ion diffusion.

We evaluate lifetimes of Li^+—G2 and Li^+—NO_3^- pairs following the approach of Borodin and Smith.[28,53] Briefly, we first compute the dimer existence autocorrelation function ($c(\tau)$, DACF). Li^+ is considered to be in a dimer with G2 precisely when the O atom of G2 is one of its six nearest neighbors. Similarly, Li^+ is in a dimer with NO_3^- precisely when the O atom of NO_3^- is one of the six nearest neighbors of Li^+. The DACF is then fit to a function of the form

$$f(\tau) = A \exp -\frac{\tau}{B} \tag{10}$$

where A and B are fitting parameters. The pair lifetime T is then

$$T = 2\int_0^\infty f(\tau)d\tau \tag{11}$$

The lifetimes are shown in Figure 7a. An increase in the NO_3^-:$TFSI^-$ ratio leads to a significant increase in the Li^+—NO_3^- lifetime (from 9.7 ns to 13.8 ns), while the lifetime of Li^+–G2 pairs decreases only slightly (from 9.7 ns to 8.2 ns). Increasing NO_3^-, not only the size and concentration of the Li^+—NO_3^- networks, but also their lifetime. This indicates that the observed ion correlations arise from both structural and dynamic aspects of Li^+ solvation.

Another important aspect to consider is the Li^+ transport mechanism. Two limiting cases are typically discussed: solvent exchange mechanism, where Li^+ hops between the coordinating solvent molecules, and vehicular transport, in which Li^+ moves together with its solvation shell.[54] The two cases are sketched in Figure 7b. In practical electrolytes, Li^+ transport generally involves a combination of both mechanisms. The relative contribution of these two mechanisms can be determined by

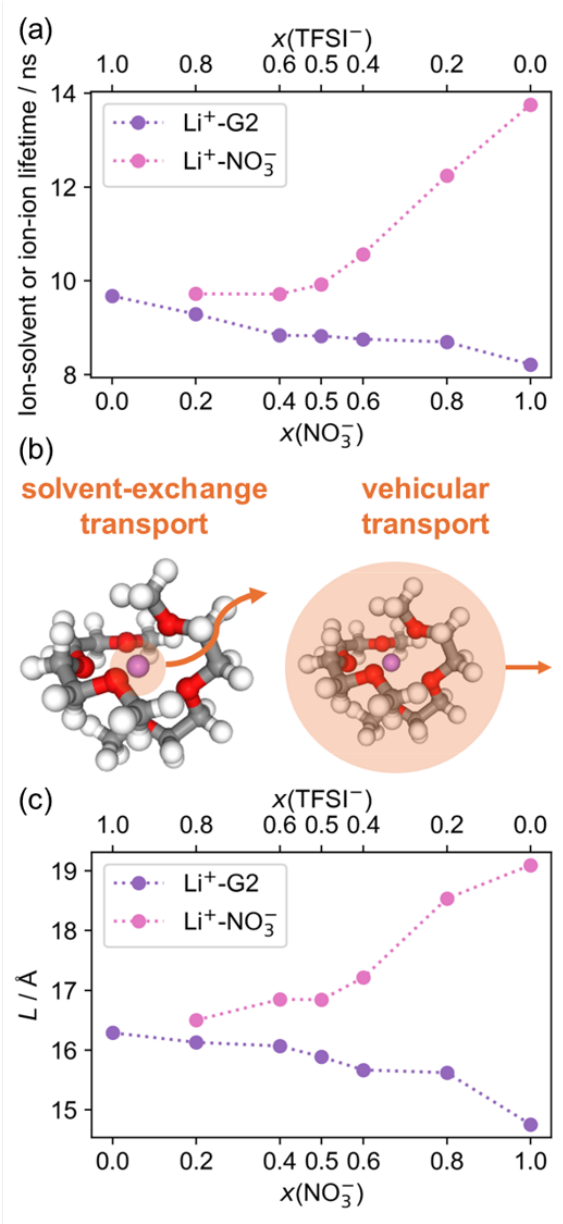

FIG. 7. **Dynamic origin of ion correlations in LiTFSI-$LiNO_3$ in G2 for different $TFSI^-$:NO_3^- ratios at fixed total molality of** 1.49 **mol kg^{-1}.** (a) Lifetime of Li^+—G2 and Li^+—NO_3^- pairs. (b) Schematic illustration of solvent-exchange and vehicular transport mechanisms of Li^+ cations through an electrolyte. (c) Characteristic length, L, for Li^+—G2 and Li^+—NO_3^- pairs. Small and large L values indicate prevalent solvent-exchange and vehicular Li^+ transport mechanisms, respectively.

evaluating the characteristic length L, defined as the average distance traveled by the Li^+ ion while coordinated with a species present in the solvation shell:[53,55]

$$L = \sqrt{6 D^{s}_{Li^+} T} \tag{12}$$

where a high L indicates vehicular-dominated transport and a low L solvent-exchange-dominated transport. Figure 7c shows the characteristic length L: as the NO_3^-:$TFSI^-$ ratio increases, the transport becomes more vehicular with respect of NO_3^- and more solvent-exchange with respect to G2. In other words, as the NO_3^- concentration increases, the distance traveled by Li^+ and NO_3^- ions while remaining coordinated also increases. This provides a clear atomistic rationale for the observed ion correlations.

Similarly, we study the solvation dynamics in the single-anion electrolytes. The Li^+—G2 and Li^+—NO_3^- lifetime (Figure S11a) increases as the $LiNO_3$ concentration increases, more rapidly for Li^+—NO_3^-. Accordingly, at the lowest $LiNO_3$ molality (0.30 mol kg^{-1}), the lifetime of Li^+—NO_3^- is lower than the Li^+—G2 lifetime, while the opposite is observed at higher concentrations. We also note that the Li^+—G2 lifetime in LiTFSI is consistently 16% to 18% longer than in $LiNO_3$, probably because the $TFSI^-$ anions do not participate significantly in the Li^+ solvation shell. Interestingly, the trend of the characteristic length, L, (Figure S11b) does not follow that of the ion-pair lifetime T, in contrast to the mixed-anion systems (Figure 7). For the $LiNO_3$ electrolytes, the Li^+—NO_3^- coordination number increases with rising $LiNO_3$ molality (Figure S9e), and similarly, the lifetime T of Li^+—NO_3^- pairs also increases (Figure S11a), suggesting a more positively correlated Li^+—NO_3^- transport. However, no increase in $D^{c}_{Li^+,NO_3^-}$ is observed (Figure S5c). Interestingly, the correlation length L shows a stronger relationship with $D^{c}_{Li^+,NO_3^-}$, indicating that the distance over which Li^+ and NO_3^- move together (reflecting the extent of vehicular transport) is more directly tied to collective diffusion behavior. This result highlights that understanding of ionic transport correlations requires not only consideration of solvation structure and ion-pair lifetimes, but also taking into account the effects on the stochastic motion of individual ions.

IV. CONCLUSIONS

In this work, we have comprehensively investigated ion transport in mixed LiTFSI-$LiNO_3$ in G2 electrolytes. As the concentration of weakly associating $TFSI^-$ ions decreases and that of strongly associating NO_3^- ions increases, the Li^+ transference number increases while the ionic conductivity decreases, similar to the behavior of highly concentrated battery electrolytes.[43] Classical MD simulations capture the experimental trend, although a polarizable force field or machine learning force fields could further improve accuracy, enabling quantitative agreement, as recently shown for conventional Li-ion battery electrolytes.[56] The observed transport characteristics are explained by strong ion-ion correlations in NO_3^--rich electrolyte formulations, arising from large and long-lived Li^+–NO_3^- ion networks. In this context, we reiterate

that an appropriate treatment of correlated ion movements in analyzing molecular simulations is essential for a reliable description of transport properties of practical battery electrolytes. We believe this work highlights a framework for systematically modulating ion transport by mixing salt anions, thereby offering a practical approach to rational electrolyte design.

ACKNOWLEDGEMENTS

Jože Grdadolnik is acknowledged for the Raman spectroscopy measurements. Bojan Šarac and Mirzet Čuskić are acknowledged for assistance with density measurements. The authors acknowledge the financial support of the Slovenian Research and Innovation Agency (ARIS) through grants P2-0423, Z2-4465, P2-0152, and I0-0039. E.R. acknowledges the France Excellence Slovénie High-Level Scientific Stay Scholarship. M.H. was funded by the European Union - NextGenerationEU (HyBReED project). The authors acknowledge the HPC RIVR consortium and EuroHPC JU for funding this research by providing computing resources of the HPC system Vega at the Institute of Information Science, Slovenia.

DATA AVAILABILITY STATEMENT

The data supporting the findings of this study will be made openly available on Zenodo after peer review.

REFERENCES

[1] B. C. Gibb, "The rise and rise of lithium," Nat. Chem. **13**, 107–109 (2021).
[2] S. Kim, G. Park, S. J. Lee, S. Seo, K. Ryu, C. H. Kim, and J. W. Choi, "Lithium-metal batteries: From fundamental research to industrialization," Adv. Mater. **35**, 2206625 (2023).
[3] A. Ponrouch, J. Bitenc, R. Dominko, N. Lindahl, P. Johansson, and M. Palacin, "Multivalent rechargeable batteries," Energy Storage Mater. **20**, 253–262 (2019).
[4] Y. S. Meng, V. Srinivasan, and K. Xu, "Designing better electrolytes," Science **378**, eabq3750 (2022).
[5] S. Ilic, S. N. Lavan, and J. G. Connell, "Anion-derived contact ion pairing as a unifying principle for electrolyte design," Chem **10**, 2987–3007 (2024).
[6] D. M. Driscoll, S. N. Lavan, M. Zorko, P. C. Redfern, S. Ilic, G. Agarwal, T. T. Fister, R. S. Assary, L. Cheng, D. Strmcnik, M. Balasubramanian, and J. G. Connell, "Emergent solvation phenomena in non-aqueous electrolytes with multiple anions," Chem **9**, 1955–1971 (2023).
[7] Y. Ko, M. A. Baird, X. Peng, T. Ogunfunmi, Y.-W. Byeon, L. M. Klivansky, H. Kim, M. C. Scott, J. Chen, A. J. D'Angelo, J. Chen, S. Sripad, V. Viswanathan, and B. A. Helms, "Omics-enabled understanding of electric aircraft battery electrolytes," Joule **8**, 2393–2411 (2024).
[8] J. He, A. Bhargav, L. Su, J. Lamb, J. Okasinski, W. Shin, and A. Manthiram, "Tuning the solvation structure with salts for stable sodium-metal batteries," Nat. Energy **9**, 446–456 (2024).
[9] J. Jiang, Q. Liu, C. Zhang, and W. Zhang, "Evaluation of acceptable charging current of power Li-ion batteries based on polarization characteristics," IEEE Trans. Ind. Electron. **61**, 6844–6851 (2014).
[10] B. D. Adams, E. V. Carino, J. G. Connell, K. S. Han, R. Cao, J. Chen, J. Zheng, Q. Li, K. T. Mueller, W. A. Henderson, and J.-G. Zhang, "Long term stability of Li-S batteries using high concentration lithium nitrate electrolytes," Nano Energy **40**, 607–617 (2017).
[11] M. Iliksu, A. Khetan, S. Yang, U. Simon, H. Pitsch, and D. U. Sauer, "Elucidation and comparison of the effect of LiTFSI and $LiNO_3$ salts on discharge chemistry in nonaqueous Li–O_2 batteries," ACS Appl. Mater. Interfaces **9**, 19319–19325 (2017).
[12] W. A. Henderson, "Glyme-lithium salt phase behavior," J. Phys. Chem. B **110**, 13177–13183 (2006).
[13] E. Jónsson and P. Johansson, "Modern battery electrolytes: Ion–ion interactions in Li^+/Na^+ conductors from DFT calculations," Phys. Chem. Chem. Phys. **14**, 10774–10779 (2012).
[14] J. Tan, M. Ye, and J. Shen, "Deciphering the role of $LiNO_3$ additives in Li–S batteries," Mater. Horiz. **9**, 2325–2334 (2022).
[15] H. Chu, J. Jung, H. Noh, S. Yuk, J. Lee, J.-H. Lee, J. Baek, Y. Roh, H. Kwon, D. Choi, K. Sohn, Y. Kim, and H.-T. Kim, "Unraveling the dual functionality of high-donor-number anion in lean-electrolyte lithium-sulfur batteries," Adv. Energy Mater. **10**, 2000493 (2020).
[16] J. Scheers, S. Fantini, and P. Johansson, "A review of electrolytes for lithium–sulphur batteries," J. Power Sources **255**, 204–218 (2014).
[17] M. Zhao, B.-Q. Li, X.-Q. Zhang, J.-Q. Huang, and Q. Zhang, "A perspective toward practical lithium–sulfur batteries," ACS Cent. Sci. **6**, 1095–1104 (2020).
[18] A. P. Thompson, H. M. Aktulga, R. Berger, D. S. Bolintineanu, W. M. Brown, P. S. Crozier, P. J. in 't Veld, A. Kohlmeyer, S. G. Moore, T. D. Nguyen, R. Shan, M. J. Stevens, J. Tranchida, C. Trott, and S. J. Plimpton, "LAMMPS - a flexible simulation tool for particle-based materials modeling at the atomic, meso, and continuum scales," Comp. Phys. Comm. **271**, 108171 (2022).
[19] J. Åqvist, "Ion-water interaction potentials derived from free energy perturbation simulations," J. Phys. Chem. **94**, 8021–8024 (1990).
[20] J. N. Canongia Lopes, J. Deschamps, and A. A. H. Pádua, "Modeling Ionic Liquids Using a Systematic All-Atom Force Field," J. Phys. Chem. B **108**, 2038–2047 (2004).
[21] B. Doherty, X. Zhong, S. Gathiaka, B. Li, and O. Acevedo, "Revisiting OPLS force field parameters for ionic liquid simulations," J. Chem. Theory Comput. **13**, 6131–6145 (2017).
[22] W. L. Jorgensen, D. S. Maxwell, and J. Tirado-Rives, "Development and testing of the OPLS all-atom force field on conformational energetics and properties of organic liquids," J. Am. Chem. Soc. **118**, 11225–11236 (1996).
[23] B. L. Bhargava and S. Balasubramanian, "Refined potential model for atomistic simulations of ionic liquid [bmim][PF_6]," J. Chem. Phys. **127**, 114510 (2007).
[24] I. Leontyev and A. Stuchebrukhov, "Accounting for electronic polarization in non-polarizable force fields," Phys. Chem. Chem. Phys. **13**, 2613–2626 (2011).
[25] Z. Li, R. Bouchal, T. Mendez-Morales, A. L. Rollet, C. Rizzi, S. Le Vot, F. Favier, B. Rotenberg, O. Borodin, O. Fontaine, and M. Salanne, "Transport properties of Li-TFSI water-in-salt electrolytes," J. Phys. Chem. B **123**, 10514–10521 (2019).
[26] L. Martínez, R. Andrade, E. G. Birgin, and J. M. Martínez, "PACKMOL: A package for building initial configurations for molecular dynamics simulations," J. Comp. Chem. **30**, 2157–2164 (2009).
[27] A. A. H. Padua, "github.com/paduagroup/fftool," (2022), (accessed 2 October 2024).
[28] M. Brehm and B. Kirchner, "TRAVIS - a free analyzer and visualizer for Monte Carlo and molecular dynamics trajectories," J. Chem. Inf. Model. **51**, 2007–2023 (2011).

[29]M. Brehm, M. Thomas, S. Gehrke, and B. Kirchner, "TRAVIS—a free analyzer for trajectories from molecular simulation," J. Chem. Phys. **152**, 164105 (2020).
[30]N. Michaud-Agrawal, E. J. Denning, T. B. Woolf, and O. Beckstein, "MDAnalysis: A toolkit for the analysis of molecular dynamics simulations," J. Comput. Chem. **32**, 2319–2327 (2011).
[31]R. J. Gowers, M. Linke, J. Barnoud, T. J. E. Reddy, M. N. Melo, S. L. Seyler, J. Domański, D. L. Dotson, S. Buchoux, I. M. Kenney, and O. Beckstein, "MDAnalysis: A Python package for the rapid analysis of molecular dynamics simulations," in *Proceedings of the 15th Python in Science Conference*, edited by S. Benthall and S. Rostrup (2016) pp. 98 – 105.
[32]O. A. Cohen, H. Macdermott-Opeskin, L. Lee, T. Hou, K. D. Fong, R. Kingsbury, J. Wang, and K. A. Persson, "Solvation-Analysis: A Python toolkit for understanding liquid solvation structure in classical molecular dynamics simulations," J. Open Source Softw. **8**, 5183 (2023).
[33]M. Salanne, "gitlab.com/ampere2/mean_square_displacements," (2023), (accessed 2 December 2024).
[34]H. Nguyen, D. A. Case, and A. S. Rose, "NGLview–interactive molecular graphics for Jupyter notebooks," Bioinformatics **34**, 1241–1242 (2017).
[35]E. Björklund, M. Göttlinger, K. Edström, D. Brandell, and R. Younesi, "Investigation of dimethyl carbonate and propylene carbonate mixtures for $LiNi_{0.6}Mn_{0.2}Co_{0.2}O_2$-$Li_4Ti_5O_{12}$ cells," ChemElectroChem **6**, 3429–3436 (2019).
[36]K. Xu, "Electrolytes and interphases in Li-ion batteries and beyond," Chem. Rev. **114**, 11503–11618 (2014).
[37]D. Bedrov, J.-P. Piquemal, O. Borodin, A. D. J. MacKerell, B. Roux, and C. Schröder, "Molecular dynamics simulations of ionic liquids and electrolytes using polarizable force fields," Chem. Rev. **119**, 7940–7995 (2019).
[38]T. Mendez-Morales, Z. Li, and M. Salanne, "Computational screening of the physical properties of water-in-salt electrolytes," Batter. Supercaps **4**, 646–652 (2021).
[39]H. Dinh Nguyen, T. Duong Pham, A. Bin Faheem, H. Min Oh, and K.-K. Lee, "Marrying a non-flammable phosphate solvent with lithium nitrate: Novel electrolyte for intrinsically safe and high performance lithium metal batteries," Batter. Supercaps **6**, e202200453 (2023).
[40]J. M. G. Barthel, H. J. Gores, R. Neueder, and A. Schmid, "Electrolyte solutions for technology - new aspects and approaches," Pure Appl. Chem. **71**, 1705–1715 (1999).
[41]F. Wohde, M. Balabajew, and B. Roling, "Li^+ transference numbers in liquid electrolytes obtained by very-low-frequency impedance spectroscopy at variable electrode distances," J. Electrochem. Soc. **163**, A714 (2016).
[42]H. Chen, K. Chen, L. Luo, X. Liu, Z. Wang, A. Zhao, H. Li, X. Ai, Y. Fang, and Y. Cao, "$LiNO_3$-based electrolytes via electron-donation modulation for sustainable nonaqueous lithium rechargeable batteries," Angew. Chem. Int. Ed. **63**, e202316966 (2024).
[43]L. Suo, Y.-S. Hu, H. Li, M. Armand, and L. Chen, "A new class of solvent-in-salt electrolyte for high-energy rechargeable metallic lithium batteries," Nat. Commun **4**, 1481 (2013).
[44]C. Park, M. Kanduč, R. Chudoba, A. Ronneburg, S. Risse, M. Ballauff, and J. Dzubiella, "Molecular simulations of electrolyte structure and dynamics in lithium–sulfur battery solvents," J. Power Sources **373**, 70–78 (2018).
[45]A. Mistry, Z. Yu, B. L. Peters, C. Fang, R. Wang, L. A. Curtiss, N. P. Balsara, L. Cheng, and V. Srinivasan, "Toward bottom-up understanding of transport in concentrated battery electrolytes," ACS Cent. Sci. **8**, 880–890 (2022).
[46]N. M. Vargas-Barbosa and B. Roling, "Dynamic ion correlations in solid and liquid electrolytes: How do they affect charge and mass transport?" ChemElectroChem **7**, 367–385 (2020).
[47]S. Pfeifer, F. Ackermann, F. Sälzer, M. Schönhoff, and B. Roling, "Quantification of cation–cation, anion–anion and cation–anion correlations in Li salt/glyme mixtures by combining very-low-frequency impedance spectroscopy with diffusion and electrophoretic NMR," Phys. Chem. Chem. Phys. **23**, 628–640 (2021).
[48]G. Horwitz, M. Factorovich, J. Rodriguez, D. Laria, and H. R. Corti, "Ionic transport and speciation of lithium salts in glymes: Experimental and theoretical results for electrolytes of interest for lithium–air batteries," ACS Omega **3**, 11205–11215 (2018).
[49]C. P. Rhodes and R. Frech, "Local structures in crystalline and amorphous phases of diglyme-$LiCF_3SO_3$ and poly(ethylene oxide)-$LiCF_3SO_3$ systems: Implications for the mechanism of ionic transport," Macromolecules **34**, 2660–2666 (2001).
[50]R. L. Frost and D. W. James, "Ion–ion–solvent interactions in solution. Part 4.—Raman spectra of aqueous solutions of some nitrates with monovalent cations," J. Chem. Soc., Faraday Trans. 1 **78**, 3235–3247 (1982).
[51]M. Castriota, T. Caruso, R. G. Agostino, E. Cazzanelli, W. A. Henderson, and S. Passerini, "Raman investigation of the ionic liquid *N*-methyl-*N*-propylpyrrolidinium bis(trifluoromethanesulfonyl)imide and its mixture with $LiN(SO_2CF_3)_2$," J. Phys. Chem. A **109**, 92–96 (2005).
[52]J. Pitawala, A. Martinelli, P. Johansson, P. Jacobsson, and A. Matic, "Coordination and interactions in a Li-salt doped ionic liquid," J. Non-Cryst. Solids **407**, 318–323 (2015).
[53]O. Borodin and G. D. Smith, "Li^+ transport mechanism in oligo(ethylene oxide)s compared to carbonates," J. Solution. Chem. **36**, 803–813 (2007).
[54]O. Borodin and G. D. Smith, "LiTFSI structure and transport in ethylene carbonate from molecular dynamics simulations," J. Phys. Chem. B **110**, 4971–4977 (2006).
[55]J. Self, K. D. Fong, and K. A. Persson, "Transport in superconcentrated $LiPF_6$ and $LiBF_4$/propylene carbonate electrolytes," ACS Energy Lett. **4**, 2843–2849 (2019).
[56]S. Gong, Y. Zhang, Z. Mu, Z. Pu, H. Wang, X. Han, Z. Yu, M. Chen, T. Zheng, Z. Wang, L. Chen, Z. Yang, X. Wu, S. Shi, W. Gao, W. Yan, and L. Xiang, "A predictive machine learning force-field framework for liquid electrolyte development," Nat. Mach. Intell. **7**, 543–552 (2025).